Folding Kinetics of a Fluorescent Variant of Monomeric λ Repressor†

Sina Ghaemmaghami, J. Michael Word, Randall E. Burton, Jane S. Richardson, and Terrence G. Oas*

Department of Biochemistry, Duke University Medical Center, Durham, North Carolina 27710

Received February 13, 1998; Revised Manuscript Received April 24, 1998

ABSTRACT: A tryptophan-containing variant of monomeric λ repressor has been made, and its folding kinetics were analyzed at 20 °C using fluorescence stopped-flow and dynamic NMR. Equilibrium denaturation curves obtained by circular dichroism, fluorescence, and NMR are superimposable. Stopped-flow analysis indicates that in the absence of denaturants the folding reaction is complete within the dead-time of the experiment. Within higher denaturant conditions, where the folding rate is slower, NMR and stopped-flow agree on the folding and unfolding rates of the protein. In 3.4 M urea and 1.8 M GdmCl, we show that the variant folds within 2 ms. Extrapolation indicates that the folding time is 20 μs in the absence of denaturants. All folding and unfolding reactions displayed monoexponential kinetics, and no burst-phases were observed. In addition, the thermodynamic parameters ΔG and m_{eq} obtained from the kinetic analysis are consistent with the equilibrium experiments. The results support a two-state D↔N folding model.

In recent years a number of small, fast-folding single domain proteins that appear to fold without the accumulation of intermediates have been identified (*1*−*8*). Collectively, these studies have cast doubt on the notion that populated intermediates along the folding pathway are obligatory for efficient folding. The folding mechanism of these proteins lacks significant kinetic traps and may be similar to early folding events of larger proteins that fold in a more complex manner. The observation that folding can occur without a distinct pathway of populated intermediates has provided support for the new view of protein folding that emphasizes multiple paths and energy landscapes over single pathways (*9*, *10*).

Although small, single domain proteins tend to fold faster than more complex proteins, their folding rate is generally within the range measurable by conventional stopped-flow instruments (<800 s^{-1}). However, at least a few of these proteins fold at speeds that challenge the limits of conventional stopped-flow, even under denaturing conditions (*7*, *8*, *11*). Dynamic NMR[1] can measure the exchange rate between two species in the sub-millisecond range and can be used to calculate the folding rate of simple, fast-folding proteins. We have previously used dynamic NMR methods to measure the folding rates of the monomeric λ repressor and its variants at 37 °C (*7*, *12*).

Monomeric λ repressor (λ_{6-85}) is a truncated form of the N-terminal domain of the bacteriophage λ cI protein (*12*). Thermodynamic studies show that the N-terminal domain folds independently of the C-terminal domain in the full-length λ repressor (*13*). Previous studies from this laboratory have shown that λ_{6-85} has the same structure in solution (*14*) as the corresponding segment in the crystal structure of the full-length protein bound to DNA (*15*). The structure consists of five α-helices interspersed with relatively short loops or turns (Figure 1). A G46A/G48A double mutation (λ^*_{6-85}) has been shown to stabilize the wild-type fragment by 1.7 kcal/mol at 37 °C (*7*, *16*, *17*). The folding kinetics of λ^*_{6-85} as studied by NMR line shape analysis indicates that it folds in 0.2 ms in 2 M urea (*7*). If no meta-stable intermediates are present at lower denaturant concentrations, this variant could fold as fast as 10 μs in the absence of urea, making it the fastest folding protein yet reported (7).

Unlike stopped-flow, NMR line shape analysis is conducted under equilibrium conditions and is therefore unable to detect folding intermediates that remain unpopulated at equilibrium under all denaturant concentrations. In this study, we have engineered a tryptophan into the core of λ^*_{6-85} in order to conduct fluorescence stopped-flow folding analysis. We show that at 20 °C the time-resolved data for λ^*_{6-85}(trp) is consistent with a kinetic two-state model, and no short-lived intermediates are observed. Accordingly, the rates measured by NMR line shape analysis and stopped-flow agree, indicating that both techniques are measuring the same kinetic event.

MATERIALS AND METHODS

Modeling of the Mutant. A computer model of λ^*_{6-85} (trp) was created from the coordinates of chain 4 (the better-ordered of the protein N-terminal domains) in the 1.8 Å Protein Data Bank entry 1LMB for the λ repressor/DNA

† This work supported by NIH Grant GM45322.

* Author to whom correspondence should be addressed. E-mail: oas@biochem.duke.edu.

[1] Abbreviations: NMR, nuclear magnetic resonance; GdmCl, guanidinium hydroochloride; CD, circular dichroism; SDS−PAGE, sodium dodecyl sulfate polyacrylamide gel electrophoresis; HPLC, high-performance liquid chromotography; λ_{6-85}, residues 6−85 of λ repressor; λ^*_{6-85}, residues 6−85 of λ repressor with G46A and G48A mutations; λ^*_{6-85}(trp), residues 6−85 of λ repressor with G46A, G48A, and Y22W mutations.

S0006-2960(98)00356-0 CCC: $15.00
Published on Web 06/06/1998

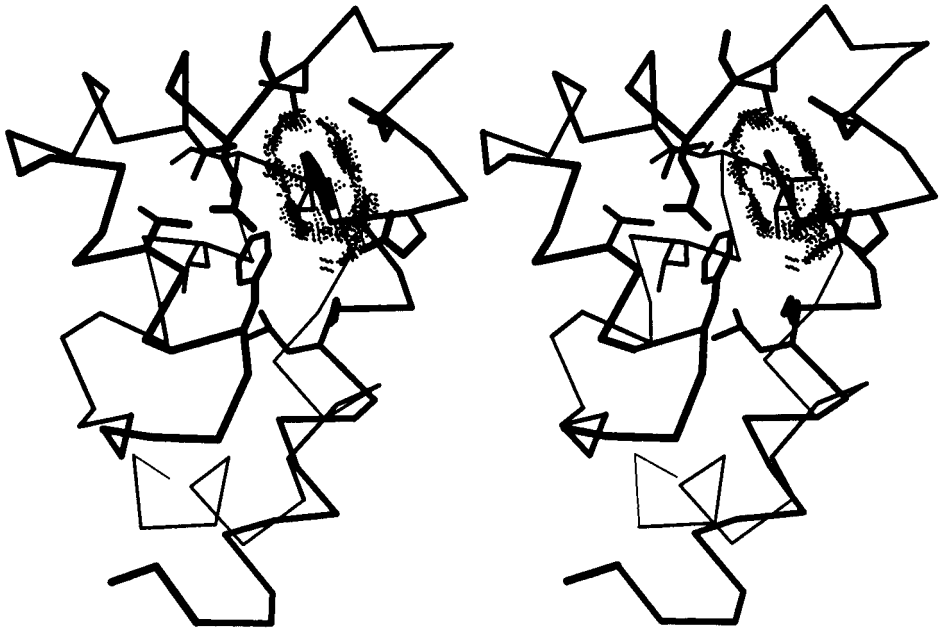

FIGURE 1: Stereo rendering of small probe contact dots for Trp22 in the model for λ^*_{6-85}(trp), with the Cα backbone and neighboring side chains, showing excellent packing of the tryptophan. A 0.25 Å radius probe was used, and dots are placed on the atomic van der Waals surface where the probe touches another nonbonded atom's VDW surface. Dot density is 16/Å^2. All H atoms (not shown) were present in the contact dot calculation.

complex (*15*). The β carbons for G46A and G48A substitutions were added using standard geometries. All hydrogens were also added in standard geometries using the program Reduce[2] (J. M. Word, unpublished). A tryptophan substitution was tried at the position of each of the aromatics (Y22, F51, Y60, and F76) and at several other buried residues (L18, V36, M40, L50, L57, L65, and L69). The Trp in each substituted model was examined using the Mage display program (*18*), rotating over a full range of side chain $\chi1$ and $\chi2$ angles to determine if there is enough room to accommodate the large side chain without significant changes to the conformation of neighboring side chains. Interactive constrained energy minimization of nearby side chains was done with Sculpt (*19*); no changes were made to the positions of backbone atoms. For the most promising conformations, small probe van der Waals contact surfaces generated with the program Probe[2] (J. M. Word, unpublished) were examined to ensure that all atoms fit favorably with their surroundings, including the interactions of all explicit H atoms. This criterion is very stringent and eliminates most candidates.

Residue 22 was considered the best candidate for substitution (Figure 1). Trp22 in the resulting λ^*_{6-85}(trp) variant packs well at $\chi1 = 174°$ and $\chi2 = 81°$— a favorable rotamer [e.g., (*20*)], with Phe51 and Lys26 contacting opposite faces of the Trp ring. Sculpt minimization made only very minor adjustments to nearby side chain positions. The conformation is very good, but the side chain NH has no hydrogen-bonding partner and the hydrophobic end of the indole ring has some solvent exposure. Comparable tryptophan conformations are observed in crystal structures, and the contact score for the new Trp in the model structure is within the top 6% found for the 279 Trp side chains in a database of 100 structures at 0.9−1.7 Å resolution (J. M. Word, unpublished).

Mutagenesis, Protein Expression, and Purification. Site-specific mutagenesis (*21*) was performed by standard single-stranded mutagenesis methods. The correct mutations were confirmed by automated DNA sequencing (generously provided by the Glaxo Wellcome Sequencing Core Facility).

The purification was conducted as previously reported (*7*), except that the protein was eluted from the AffiGel Blue column using 4 M KCl and the G-50 column was run with water instead of 5% acetic acid. The homogeneity of the purified product was verified with SDS−PAGE, HPLC, and mass spectrometry.

Circular Dichroism and Fluorescence Spectra. The CD spectra were recorded at a concentration of ∼100 μM in 100 mM NaCl, 20 mM potassium phosphate (pH 8.0) at 20 °C on an Aviv 62DS spectropolarimeter. The spectra of the denatured proteins were collected in the presence of 9 M urea. The exact protein concentrations were determined by UV absorbance. The signal at each wavelength was averaged for sixty seconds and the spectra were corrected for baseline contribution of the buffer before being converted to mean residual ellipticity. The fluorescence emission spectra were measured at a concentration of ∼1 μM in the same buffer at 20 °C with and without 9 M urea. An Aminco Bowman Series 2 Luminescence spectrophotometer and 1 cm path length cuvettes were used. The excitation wavelength was 290 nm.

Equilibrium Denaturation Curves. The buffer used for all experiments consisted of 100 mM NaCl, 20 mM potassium phosphate (pH 8.0). For CD experiments, samples of both λ^*_{6-85} and λ^*_{6-85}(trp) were made at concentrations of approximately 10 μM measured exactly by UV absorbance. The CD signal was monitored at 222 nm on an Aviv 62DS spectropolarimeter equipped with a Hamilton syringe titration apparatus. All measurements were conducted at 20 °C. The

[2] The programs Reduce, Probe, Prekin, and Mage are available at ftp://suna.biochem.duke.edu/pub/UNIXprograms.

proteins were incrementally titrated with a high denaturant concentration stock solution whose concentration was determined by refractive index measurements to within ±0.01 M. Fluorescence titration was conducted similarly with 2 μM λ^*_{6-85}(trp) solution, except that the titration was conducted manually. The excitation wavelength was 290 nm, and emission wavelength was 320 nm. All titration curves were fit using the two-state equation (*22*).

NMR line shape analysis. λ^*_{6-85}(trp) solutions of approximately 500 μM were made in different concentrations of urea in 100 mM NaCl, 20 mM potassium phosphate (pH 8.0) in D_2O. The final concentrations of protein and urea were determined by UV absorbance and refractometry, respectively. ^{1}H NMR spectra were recorded on a Varian Unity 500 MHz spectrometer with water and urea presaturation at 20 °C. The aromatic spectra (3000 to 4000 Hz, from TMSP) in the transition region were fitted as described previously (*7*, *23*).

Fluorescence Stopped-Flow. A DX.17MV sequential mixing stopped-flow spectrophotometer from Applied Photophysics was used. The path length of the cell was 2 mm. Excitation was at 290 nm and emission was followed using a 10 nm bandwidth filter at 320 nm. The dead-time was measured under all experimental conditions using the test reaction between 2,6-dichlorophenolindophenol and L-ascorbate (*24*). The dead-times ranged from 2.0 to 4.2 ms depending on the denaturant concentration and pneumatic pressure used. All reactions were conducted at 20 °C. Urea and GdmCl folding reactions were initiated by an 11-fold dilution of 9 M urea or 4 M GdmCl protein solutions into lower denaturant concentrations to give the desired final concentration. Unfolding reactions were conducted similarly by 11-fold dilution of 0 M denaturant solutions into higher denaturant conditions. The final concentration of protein was ~25 μM. The resulting folding and unfolding traces were fit using the following equation in Kaleidagraph (Synergy Software):

$$S(t) = S_f + (S_i - S_f)e^{-k_{app}t} \quad (1)$$

where S_f is the final signal, S_i is the initial signal, k_{app} is the rate constant, t is time, and $S(t)$ is signal as a function of time.

The amplitudes were measured by subtracting the final fluorescence signal from the initial fluorescence signal at time zero (as determined by the dead-time calculation). The logarithms of the observed rates were plotted as a function of denaturant and fitted to the following equation according to a two-state model:

$$k_{app} = k_u + k_f \quad (2)$$

where

$$k_u = e^{(\ln k_u^o + m_u C)} \quad (3)$$

$$k_f = e^{(\ln k_f^o + m_f C)} \quad (4)$$

k_u and k_f are the unfolding and folding rate constants which depend exponentially on the denaturant concentration. C is the concentration of denaturant, k_f^o and k_u^o are the folding and unfolding rate constants in the absence of denaturant, and m_f and m_u are the slopes of their denaturant dependence. The α parameter, $\Delta G°$, and m_{eq} are related to the kinetic data as shown in eqs 6−8:

$$\Delta G° = -RT\ln\left(\frac{k_u^o}{k_f^o}\right) \quad (5)$$

$$m_{eq} = RT(m_f + m_u) \quad (6)$$

$$\alpha = \frac{m_u}{m_u - m_f} \quad (7)$$

The fits of the chevron plots were conducted using the following equation derived from the above relationships:

$$k_{app} = k_f^o(e^{[m_{eq}(-1+\alpha)C]/RT} + e^{(\Delta G° + \alpha m_{eq}C)/RT}) \quad (8)$$

N-Acyl-tryptophan-amide Controls. A 1.33 μM solution of *N*-acyl-trp-amide was titrated with urea and GdmCl as described above. Its fluorescence emission at 350 nm was followed with an excitation wavelength of 280 nm. The urea titration resulted in a linear function with a slope of 0.1 (the fluorescence doubles by the addition of 10 M urea) and the GdmCl titration resulted in a linear function with a slope of 0.01 (fluorescence increases by 5% by the addition of 5 M GdmCl). Stopped-flow experiments were conducted with *N*-acyl-trp-amide as stated above with final concentration of 2.5 μM. For urea refolding experiments, a significant decrease in fluorescence occurred within the dead-time of the experiment, in accordance with the titration results. For GdmCl refolding experiments, this decrease was negligible. No other folding artifacts were observed.

RESULTS

Construction of the Model and Spectroscopic Characterization. A tyrosine was mutated to a tryptophan at position 22 in λ^*_{6-85} in order to provide a fluorescent probe for the folding of the protein [λ^*_{6-85}(trp)]. Position 22 was chosen for the Trp insertion in the core as it leads to the least disturbance in the structure of the protein according to computer modeling(Figure 1). The mutation does not significantly alter the far UV CD spectrum (Figure 2a), suggesting that the structure of the protein has not been drastically altered. The change in the near UV CD spectrum confirms the presence of tryptophan and suggests that the slight difference between the spectra in the far UV region is probably due to the presence of the indole side chain. The stability of the protein is not changed significantly by the mutation, increasing by 0.2 kcal/mol which is within the error of the experiment (data not shown). The fluorescence spectra of the λ^*_{6-85}(trp) with excitation at 290 nm in the presence of 0 and 9 M urea are shown in Figure 2b. There is a blue shift of 20 nm and a slight increase in intensity upon folding. The greatest intensity difference between the two states is at 320 nm. Fluorescence emission at this wavelength was used as the probe for folding.

Equilibrium Denaturation. The equilibrium unfolding of λ^*_{6-85}(trp) was examined by the addition of urea and GdmCl at 20 °C. The CD signal at 222 nm and the fluorescence emission at 320 nm upon excitation at 290 nm were monitored. The fluorescence and CD denaturation curves shown in Figure 4 are superimposable, suggesting that the

Table 1: Comparison of Thermodynamic Folding Parameters of λ^*_{6-85}(trp) Derived from Equilibrium and Kinetic Analyses

method	denaturant	ΔG_{min}[b] (kcal/mol)	ΔG°[c] (kcal/mol)	m_{eq} (kcal mol^{-1} M^{-1})
equilibrium CD	urea	2.5 ± 0.1	5.9 ± 0.2	0.99 ± 0.04
equilibrium fluorescence	urea	2.4 ± 0.1	5.8 ± 0.3	1.03 ± 0.07
equilibrium CD	GdmCl	1.6 ± 0.1	5.6 ± 0.2	2.17 ± 0.08
equilibrium fluorescence	GdmCl	1.6 ± 0.1	5.6 ± 0.2	2.20 ± 0.08
NMR line shape analysis	urea	2.3 ± 0.2	5.6 ± 0.3	1.05 ± 0.05
stopped-flow fluorescence	urea	2.1 ± 0.2	5.7 ± 0.3	1.03 ± 0.04
stopped-flow fluorescence	GdmCl	1.6 ± 0.2	5.5 ± 0.3	2.2 ± 0.1

[a] Experimental equilibrium data derived from two-state analysis of the titration curves (Figure 3). Stopped-flow data derived from the analysis of chevron plots (Figure 4). [b] ΔG_{min} determined at the lowest denaturant concentrations where folding could be measured by stopped−flow (3.4 M urea and 1.8 M GdmCl). [c] Kinetic data could not be collected at low denaturant concentrations and therefore the kinetically derived thermodynamic parameters in water are based on extrapolation. See Materials and Methods and text for details.

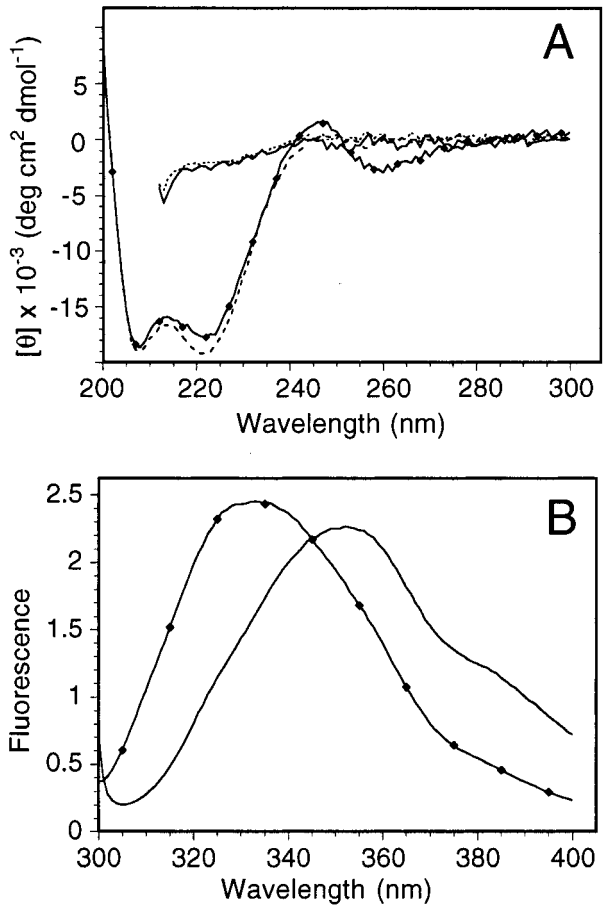

FIGURE 2: Circular dichroism (A) and fluorescence emission (B) spectra of folded and unfolded λ^*_{6-85} and λ^*_{6-85}(trp). All measurements were conducted at 20 °C in 100 mM NaCl, 20 mM potassium phosphate (pH 8.0). Folded spectra were obtained in 9 M urea, and unfolded spectra were obtained in buffer alone. For fluorescence, the excitation wavelength was at 290 nm. λ^*_{6-85}(trp) folded (−◆−), λ^*_{6-85}(trp) unfolded (−), λ^*_{6-85} folded (− − −), λ^*_{6-85} unfolded (- - -).

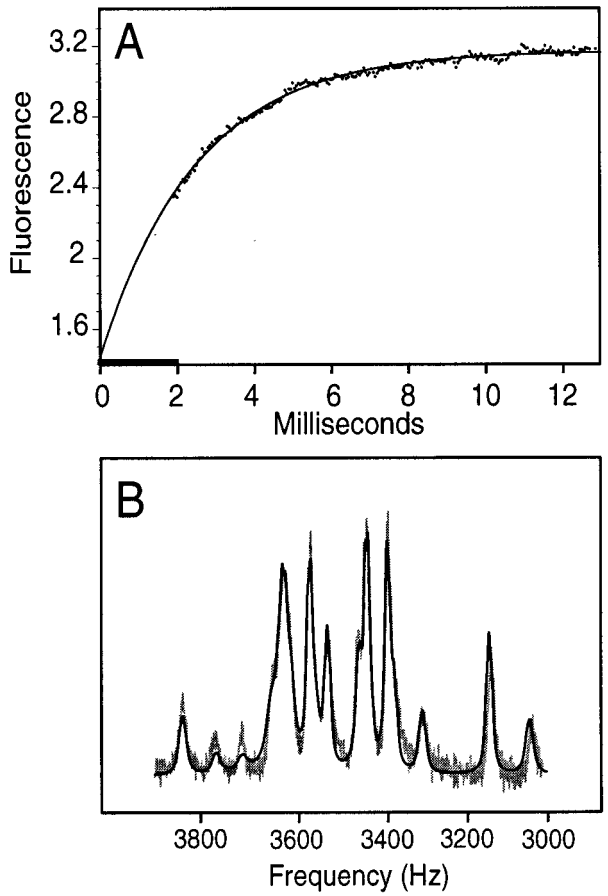

FIGURE 3: (A) Stopped-flow folding trace for λ^*_{6-85}(trp) following a jump from 9.0 M urea to 3.4 M urea. The solid line is the fit to a single-exponential equation. The measured rate constant was 450 s^{-1}. The bar on the *x*-axis indicates the dead-time of the experiment. All other traces were also fit well to single-exponential equations. Lower final urea concentrations resulted in reactions which were completed within the dead-time of the experiment. (B) Experimental and simulated aromatic ^{1}H NMR spectra for λ^*_{6-85}(trp) at 4.8 M urea. Experimental data are shown in gray and the best-fit simulation is shown as a solid line. The measured exchange rate constant was 108 s^{-1}. All other spectra in the transition region were similarly well fit with our simulations. Experiments were performed at 20 °C in 100 mM NaCl, 20 mM potassium phosphate (pH 8.0).

loss of secondary and tertiary structure occur concurrently. The simple D↔N folding model was applied to the titration curves (see Materials and Methods), and the ΔG° and m_{eq} values were measured (Table 1). These superimposable denaturation curves, along with those determined previously by NMR for wild-type λ_{6-85} (*14*), strongly suggest that only two states (folded and unfolded) are significantly populated under any given denaturant concentration when equilibrium is reached. λ^*_{6-85} can thus be thought of as a *thermodynamically* two-state system.

NMR Line Shape Analysis. Because the folding of λ^*_{6-85}(trp) involves only two equilibrium-populated states in the transition region of the urea titration curve, the shape of the NMR ^{1}H-spectra are a function of (a) the relative population of each state, (b) the urea-dependent spectrum of each state, and (c) the rate which the two states are chemically exchanging. We have previously shown that these variables are sufficiently independent to be defined uniquely by the ^{1}H aromatic spectrum of the protein (*7*, *25*). Figure 3a shows an example of a typical simulated spectrum

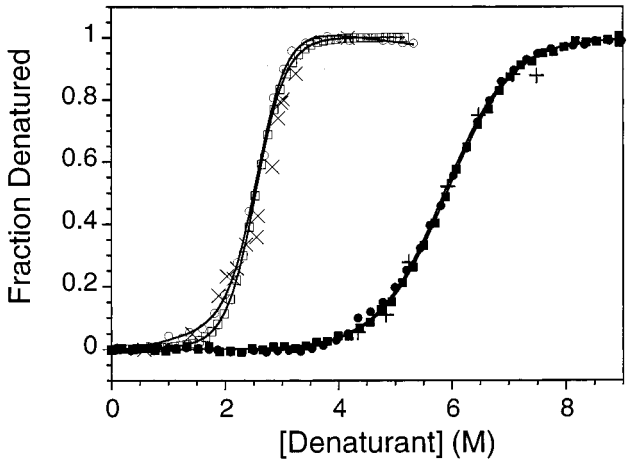

FIGURE 4: Comparison of fraction denatured calculations for λ^*_{6-85}(trp) by equilibrium and kinetic techniques. Equilibrium titration as monitored by CD at 220 nm: GdmCl as denaturant (□), urea as denaturant (■). Equilibrium titration as monitored by fluorescence: GdmCl as denaturant (○), urea as denaturant (●). Superimposed are the fraction denatured as measured by NMR line shape analysis (+) and as measured by fractional amplitude of the stopped-flow traces (×). Experiments were performed at 20 °C in 100 mM NaCl, 20 mM K_2PO_4 (pH 8.0). The titration curves were fit to a two-state equation as described in Materials and Methods (solid lines).

based on the above rationale, superimposed on the actual spectrum of the aromatic region of λ^*_{6-85}(trp) at 5.2 M urea. The agreement between the simulated and observed data under all measured urea concentrations supports our conclusions about the thermodynamically two-state nature of the transition region as the entire aromatic spectrum can be defined as a function of just two spectra (folded and unfolded) and one exchange rate. NMR line shape analysis also provides an independent measure of the population ratio of each state at various urea concentrations. Figure 4 shows the fraction denatured calculated by this analysis superimposed on the equilibrium titration curves, and Table 1 compares the m_{eq} and $\Delta G°$ values measured by the two methods. The close agreement between the thermodynamic parameters obtained by NMR line shape analysis and equilibrium titration curves provides further support for our thermodynamically two-state model.

Urea Stopped-Flow. The above equilibrium-based observations do not rigorously rule out the existence of folding intermediates in the folding pathway. For example, proteins that have a populated transient intermediate only at low denaturant concentrations (where the population as a whole is dominated by the native state) would still display superimposable titration curves which are fit well by thermodynamic two-state assumptions. To provide evidence against the existence of transient intermediates, folding must be analyzed in a time-resolved manner. The following three observations are generally required for a *kinetically* two-state system (*1*): (a) monophasic folding under all urea concentrations, (b) a chevron-shaped plot of log of folding rate against urea concentrations as defined by two-state assumptions (see Materials and Methods), and (c) the agreement between kinetically and equilibrium derived folding parameters.

The change in fluorescence of λ^*_{6-85}(trp) upon folding allows detection of the folding reaction transiently using a stopped-flow apparatus. Transient intermediates that do not accumulate at equilibrium and are therefore invisible to NMR line shape analysis can be detected by monitoring the reaction in a time-resolved manner with stopped-flow. Stopped-flow studies of λ^*_{6-85}(trp) refolding and unfolding reactions conducted at different final urea concentrations displayed traces that were well fit by monoexponential equations under all conditions. The fastest folding trace whose rate could be accurately measured by stopped-flow (at 3.4 M urea) is shown in Figure 3b and is typical of all observed traces. Final urea concentrations below 3.4 M resulted in a folding reaction that was complete within the dead-time of the instrument.

GdmCl Stopped-Flow. Many previously studied proteins display an early fast-folding phase that is complete within the dead-time of the stopped-flow experiment (*26*, *27*). Such burst-phases can be detected by the observation that the extrapolation of the exponentially fitted kinetic traces to the dead-time of the instrument does not correspond to the signal at initial conditions of the experiment. This analysis is somewhat complicated when urea is used as a denaturant because of the strong urea dependence of tryptophan fluorescence (*5*). This effect can be observed as a relatively sharp slope of the denatured baseline in the raw fluorescence titration curve (not shown). A similar effect is also seen when N-acyl-tryptophan amide is titrated with urea (see Materials and Methods). For this reason, the estimation of the initial fluorescence of each unfolding and refolding stopped-flow experiment requires careful extrapolation from native and denatured baselines, respectively. Due to the stability of λ^*_{6-85}(trp), the denatured baseline of the urea titration curve is not defined very clearly and such an extrapolation is error-prone. GdmCl, on the other hand, does not strongly affect the fluorescence of tryptophan as indicated by the low GdmCl dependence of the λ^*_{6-85}(trp) denatured baseline and the flat *N*-acyl-trp-amide titration curve (see Materials and Methods). We therefore repeated the stopped-flow experiments using GdmCl as a denaturant to detect a possible burst-phase. All unfolding and refolding experiments were again well fitted by single-exponential equations. Final GdmCl concentrations below 1.8 M resulted in folding reactions that were completed within the dead-time of the instrument. Fraction amplitude at each GdmCl concentration was measured by dividing the total amplitude of the kinetic trace (taking into account the dead-time) by the total amplitude between the folded and unfolded states (0 M GdmCl and 4 M GdmCl, respectively). Figure 3 shows a plot of the fraction denatured as measured by the fluorescence titration curve superimposed on a plot of fraction amplitudes of the fitted stopped-flow traces as a function of GdmCl. The entire fluorescence changes observed under equilibrium conditions are accounted for by the amplitudes of our monoexponential reactions at all observable GdmCl concentrations. This observation suggests that (a) there is no burst-phase present and (b) the entire reaction is complete, and no subsequent slower phase exists.

Denaturant Dependence of Folding Rates. Traces that were more than 60% complete after the dead-time and those whose amplitudes were less than ~10% of the total amplitude between the folded and unfolded states could not be fit with sufficient accuracy for their rates to be measured. All measurable traces were fit to a single-exponential equation

Table 2: Kinetic Folding Parameters of λ^*_{6-85}(trp) Derived from NMR and Stopped-Flow Techniques[a]

method	denaturant	$k_f^{ob} \times 10^{-3}$ (s^{-1})	k_u^{ob} (s^{-1})	$k_{f,min}$[c] (s^{-1})	$k_{u,min}$[c] (s^{-1})	m_f (kcal mol^{-1} M^{-1})	m_u (kcal mol^{-1} M^{-1})
NMR line shape analysis	urea	28 ± 16	2.0 ± 1.0	510 ± 40	11 ± 1	-1.20 ± 0.10	0.50 ± 0.05
stopped-flow fluorescence	urea	61 ± 18	3.6 ± 1.0	450 ± 30	12 ± 3	-1.40 ± 0.05	0.35 ± 0.09
stopped-flow fluorescence	GdmCl	62 ± 48	5.0 ± 1.1	470 ± 30	32 ± 9	-2.70 ± 0.15	1.00 ± 0.30

[a] Kinetic parameters derived from the analysis of the chevron plot (Figure 4) as described in Materials and Methods. [b] Rate constants in the absence of denaturant, based on extrapolation. [c] k_{min} at the lowest denaturant concentrations where folding could be measured by stopped−flow (3.4 M urea and 1.8 M GdmCl). See Materials and Methods and text for details.

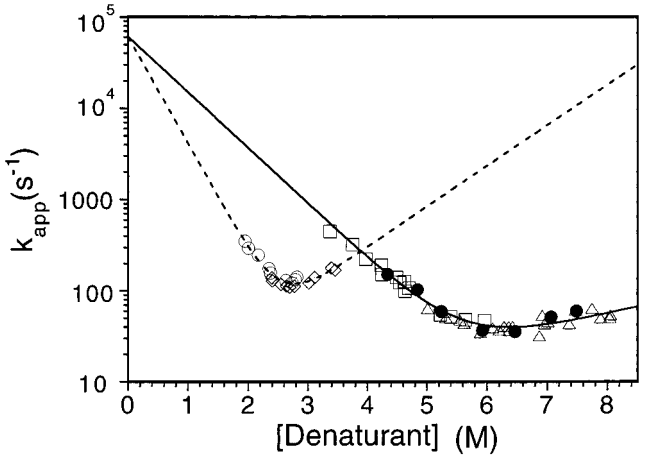

FIGURE 5: Dependence of the folding and unfolding kinetics obtained by stopped-flow and NMR line shape analysis on the denaturant concentration. Stopped-flow reactions were conducted in GdmCl (refolding (○), unfolding (◇), and urea (re-folding □, unfolding (△). The data were fitted according to a two-state model as described in Materials and Methods. Superimposed are the kinetic measurements by NMR line shape analysis in urea (●). Experiments were performed at 20 °C in 100 mM NaCl, 20 mM K_2PO_4 (pH 8.0).

(see Materials and Methods), and their k_{app}'s were determined. Figure 5 shows the plot of log k_{app} versus denaturant concentration for both urea and GdmCl at concentrations where the rate could be measured accurately. The apparent rate constants at high denaturant concentrations were measured by unfolding experiments, whereas those at low denaturant concentrations were determined by refolding experiments. In the transition region, where the k_{app} could be measured by both folding and unfolding experiments the two rates agree, consistent with the kinetic two-state model. The chevron-shaped plot is consistent with a kinetically two-state mechanism within observable denaturant concentrations (3.4−9 M urea and 1.8−4 M GdmCl) and does not deviate from linearity within this range. Also, both urea and GdmCl dependences show similar extrapolated folding and unfolding rates at 0 M denaturant concentration (Figure 5). Tables 1 and 2 list the thermodynamic and kinetic parameters derived from equilibrium denaturation curves and stopped-flow analysis. The close agreement between the data supports the kinetic two-state model within the range of denaturant concentrations that resulted in measurable folding rates.

Also shown in Figure 4 is the plot of the log of the measured exchange rates ($k_f + k_u$) as a function of urea concentration as determined by NMR line shape analysis. This plot is also well fit by the two-state equation and is superimposable with the stopped-flow chevron plot. The strong agreement between the two methods confirms that the line-broadening observed in our NMR analysis is indeed due to the complete folding and unfolding of the protein. It also suggests that the two methods can measure folding rates with similar accuracies.

DISCUSSION

Current views on how proteins fold are strongly influenced by kinetic, in vitro folding studies of model proteins. Although many model systems have been studied, the kinetic techniques being used to study them are limited in number. Stopped-flow is the most commonly used technique, but its dead-time of ~1 ms makes it useful only for reactions slower than ~800 s^{-1}. Our previous studies had shown that dynamic NMR can be used to measure submillisecond folding rates for the monomeric λ repressor and its variants. In this study we demonstrate that this technique is consistent with conventional stopped-flow methods. We have engineered a tryptophan into a thermostable variant of monomeric λ repressor to allow fluorescence detected stopped-flow experiments. The fast folding rate of the protein does not allow folding experiments in low denaturant concentrations. At higher denaturant conditions the data are consistent with a simple two-state model, and the rates measured by stopped-flow and NMR agree.

The results obtained by NMR line shape analysis and fluorescence stopped-flow are consistent with a simple D↔N model within observable denaturant concentrations. The equilibrium and dynamic NMR studies suggest that λ^*_{6-85}(trp) is a thermodynamically two-state system with no equilibrium-populated intermediates. The stopped-flow analysis provides evidence that our system is also a kinetically two-state system with no intermediates accumulating transiently within the course of the reaction.

Neither stopped-flow nor NMR line shape analysis can measure the folding rates of λ^*_{6-85}(trp) at low denaturant conditions for this protein. Under these conditions, folding rates surpass the experimental limit of the stopped-flow instrument, and the unfolded state is not sufficiently populated at equilibrium for dynamic NMR. Hence, to calculate folding rates in the absence of denaturant, a considerable linear extrapolation is necessary. This linear extrapolation would be valid if folding remains two-state at lower denaturant conditions. However, some proteins have been shown to have transiently populated intermediates at low denaturant concentrations that are destabilized at higher denaturant concentrations and a nonlinear log folding rate vs denaturant concentration plot is observed (*28*, *29*). Both dynamic NMR and stopped-flow at higher denaturant conditions would be blind to the presence of such an intermediate. This scenario would make our extrapolation an overestimation of the rate of folding in the absence of denaturant. However, if such an intermediate exists for λ^*_{6-85}(trp) it must be relatively unstable since at 1.8 M GdmCl and 3.4 M urea it has become completely destabilized and is not transiently populated.

A previous concern about the dynamic NMR method as applied to protein folding was the possibility that the observed line-broadening is due to chemical exchange between the native state and a precollapsed intermediate that folds much faster than the chemically denatured protein. Here, we have shown that within the regimes measurable by both stopped-flow and NMR line shape analysis, the two techniques agree on the folding rates of the protein. These results, in addition to the observation that the equilibrium constants obtained from the NMR method match the equilibrium titration data obtained by CD, strongly suggest that the line broadening in the NMR spectra is due to the complete folding reaction. The close agreement between the rates measured by the two techniques also provides evidence that the dynamic NMR method can measure folding rates with at least the same accuracy as a typical stopped-flow experiment.

Stopped-flow and NMR line shape analysis have several complimentary advantages and limitations. (1) Stopped-flow requires a convenient spectroscopic probe such as a buried tryptophan residue or a large change of the CD signal upon folding, whereas NMR line shape analysis requires a well dispersed and easily assignable region in the ^{1}H NMR spectrum. (2) Stopped-flow cannot typically measure rates faster than 800 s^{-1}, whereas NMR line shape analysis of λ^*_{6-85}(trp) can measure rates as fast as 10^6 s^{-1} (*7*). (3) The lower limit for the final denaturant concentration for a stopped-flow experiment is determined by the degree of dilution allowed by the instrument (typically 10% of the initial denaturant concentration), whereas no such limit exists for NMR line shape analysis. (4) NMR line shape analysis can only be used under conditions where both the folded and unfolded states are partially populated at equilibrium (transition region), whereas the final denaturant conditions of a stopped-flow experiment are not limited by the equilibrium populations.

The agreement of the two techniques suggests that one can alternate between the two methods depending on which is more advantageous for a particular protein under the desired experimental conditions. In particular, two-state proteins which fold rapidly (faster than the limits of stopped-flow) and yet are relatively unstable (so that the unfolded state is somewhat populated at lower denaturant conditions) are ideal for the NMR technique. Line shape analysis would also be favored at higher temperatures which tend to increase the folding rate while destabilizing the protein.

In conclusion, stopped-flow and dynamic NMR analysis of λ^*_{6-85}(trp) confirm the two-state nature of its folding mechanism (at least within higher denaturant conditions), and the results indicate that λ^*_{6-85}(trp) folds in the submillisecond range at 20 °C. Also, the close agreement with stopped-flow validates dynamic NMR as an accurate kinetic technique and suggests that it can be a valuable tool in studying fast-folding, two-state proteins.

REFERENCES

1. Jackson, S. E., and Fersht, A. R. (1991) *Biochemistry 30*, 10428−35.
2. Alexander, P., Orban, J., and Bryan, P. (1992) *Biochemistry 31*, 7243−7248.
3. Viguera, A. R., Martinez, J. C., Filimonov, V. V., Mateo, P. L., and Serrano, L. (1994) *Biochemistry 33*, 2142−2150.
4. Kragelund, B. B., Robinson, C. V., Knudsen, J., Dobson, C. M., and Poulsen, F. M. (1995) *Biochemistry 34*, 7217−7224.
5. Schindler, T., Herrler, M., Marahiel, M. A., and Schmid, F. X. (1995) *Nat. Struct. Biol. 2*, 663−673.
6. Villegas, V., Azuaga, A., Catasus, L., Reverter, D., Mateo, P. L., and Serrano, L. (1995) *Biochemistry 35*, 15105−15110.
7. Burton, R. E., Huang, G. S., Daugherty, M. A., Fullbright, P. W., and Oas, T. G. (1996) *J. Mol. Biol. 263*, 311−322.
8. Robinson, C. R., and Sauer, R. T. (1996) *Biochemistry 35*, 13878−13884.
9. Wolynes, P. G., Onuchic, J. N., and Thirumalai, D. (1995) *Science 267*, 1619−1620.
10. Dill, K. A., and Chan, H. S. (1997) *Nat. Struct. Biol. 4*, 10−19.
11. Bai, Y., Karimi, A., Dyson, J., and Wright, P. E. (1997) *Protein Sci. 6*, 1449−1457.
12. Huang, G. S., and Oas, T. G. (1995) *Proc. Natl. Acad. Sci. U.S.A. 92*, 6878−6882.
13. Sauer, R. T., Jordan, S. R., and Pabo, C. O. (1990) *Adv. Protein Chem. 40*, 1−61.
14. Huang, G. S., and Oas, T. G. (1995) *Biochemistry 34*, 3884−3892.
15. Beamer, L. J., and Pabo, C. O. (1992) *J. Mol. Biol. 227*, 177−196.
16. Hecht, M. H., Hehir, K. M., Nelson, H. C., Sturtevant, J. M., and Sauer, R. T. (1985) *J. Cell. Biochem. 29*, 217−24.
17. Hecht, M. H., Sturtevant, J. M., and Sauer, R. T. (1986) *Proteins 1*, 43−6.
18. Richardson, D. C., and Richardson, J. S. (1992) *Protein Sci. 1*, 3−9.
19. Surles, M. C., Richardson, J. C., Richardson, D. C., and Brooks, F. P. (1994) *Protein Sci. 3*, 198−210.
20. Ponder, J. W., and Richards, F. M. (1987) *J. Mol. Biol. 193*, 775−791.
21. Kunkel, T. A., Roberts, J. D., and Zakour, R. A. (1987) *Methods Enzymol. 154*, 367−382.
22. Pace, C. N. (1986) *Methods Enzymol. 131*, 266−280.
23. Burton, R. E., Busby, R. S., and Oas, T. G. (1998) *J. Biomol. NMR* (in press).
24. Tonomura, B., Nakatani, H., Ohnishi, M., Yamaguchi-Ito, J., and Hiromi, K. (1978) *Anal. Biochem. 84*, 370−383.
25. Huang, G. S., and Oas, T. G. (1995) *Proc. Natl. Acad. Sci. U.S.A. 92*, 6878−6882.
26. Khorasanizadeh, S., Peters, I. D., and Roders, H. (1996) *Nat. Struct. Biol. 3*, 193−205.
27. Raschke, T. M., and Marquesee, S. (1997) *Nat. Struct. Biol. 4*, 298−304.
28. Khorasanizadeh, S., Peters, I. D., Butt, T. R., and Roder, H. (1993) *Biochemistry 32*, 7054−63.
29. Matouschek, A., Matthews, J. M., Johnson, C. M., and Fersht, A. R. (1994) *Protein Eng. 7*, 1089−1095.

BI980356B